JOURNAL OF COMPUTATIONAL PHYSICS 91, 361–380 (1990)

A Three-Dimensional Lagrangian Method for Fluid Dynamics

L. BILBAO*

Laboratorio de Fisica del Plasma - FCEN, Universidad de Buenos Aires, Ciudad Universitaria - Pab. I, 1428 Buenos Aires, Argentina

Received September 6, 1988; revised May 30, 1989

Using six-surfaced cells the space-derivative terms in the Lagrangian equations are reduced to simple algebraic expressions, that require volume and surface variables. In order to preserve the thermodynamic relation for internal energy for each cell, the surface magnitudes are chosen from the neighbor cells in the following way: the velocity from the volume velocity of the cell "ahead" while the pressure from the volume pressure of the cell "behind." Together with a simple predictor-corrector scheme a stable (Courant number 0.5) and fast code may be written. Although it is less accurate than other methods, it exhibits some interesting features: it retains the advantages of sided methods for imposing boundary conditions, and it preserves the simplicity of the explicit schemes (a fact particularly useful to vectorize it).

1. INTRODUCTION

For solving multidimensional problems several numerical methods are based on a network of deformable volume elements (usually a six-surfaced cell in 3D problems). Among these kinds of multidimensional codes are: YAQUI [1] in 2D, and BAAL [2] or SALE-3D [3] for 3D problems. In all these codes velocities are assigned to the cell vertices while pressure, density, etc. are centered. When a surface value is needed, an appropriate mean value over two or more adjacent cells is calculated. In this work a method that uses values from only one neighbor cell (but a different cell for a different variable) is reported. The assignment is done in such a way that an underlying physical principle of compressible fluids is preserved: the thermodynamics relation for internal energy.

2. SEMIDISCRETE EQUATIONS

Let us consider an inviscid compressible fluid. Integrating the Euler equations over a volume V whose surface S is moving with the fluid (Lagrangian formulation) we get

$$\frac{dM}{dt} = 0 \tag{1}$$

* Member of Carrera del Investigador Cientifico del CONICET (Argentina).

0021-9991/90 $3.00

581/91/2-8

$$\frac{d\mathbf{P}}{dt} = -\oint d\mathbf{S}\, p \tag{2}$$

$$\frac{dU}{dt} = -\oint d\mathbf{S} \cdot \mathbf{v}\, p, \tag{3}$$

where M, $\mathbf{P}$, and U are the total mass, momentum, and energy contained within $\mathbf{S}$ at time t, $\mathbf{v}$ is the velocity, and p the pressure ($d\mathbf{S}$ is outward from V). Accordingly, the evolution of V is written

$$\frac{dV}{dt} = \oint d\mathbf{S} \cdot \mathbf{v}. \tag{4}$$

For a three-dimensional flow we shall use the following conventions:

— The cell (i, j, k) is the volume element limited by the vertices $(i-\frac{1}{2}, j-\frac{1}{2}, k-\frac{1}{2})$, $(i+\frac{1}{2}, j-\frac{1}{2}, k-\frac{1}{2})$, etc. (see Fig. 1) in the logical coordinate space (ξ, η, ζ) [4].

— Vertices are numbered from 1 to 8 according to Fig. 2.

— The six sides of each hexahedral cell are named with the letters a through f (see Fig. 2).

— For numerical convenience $\mathbf{S}_a$, $\mathbf{S}_b$, and $\mathbf{S}_c$ are chosen inward to V, while $\mathbf{S}_d$, $\mathbf{S}_e$, and $\mathbf{S}_f$ are outward from V, i.e.,

$$\mathbf{S}_a = \tfrac{1}{2}(\mathbf{r}_7 - \mathbf{r}_1) \times (\mathbf{r}_5 - \mathbf{r}_3) \tag{5.1}$$

$$\cdots \qquad \cdots$$

$$\mathbf{S}_d = \tfrac{1}{2}(\mathbf{r}_8 - \mathbf{r}_2) \times (\mathbf{r}_6 - \mathbf{r}_4) \tag{5.4}$$

$$\cdots \qquad \cdots$$

where $\mathbf{r}$ is the physical coordinate.

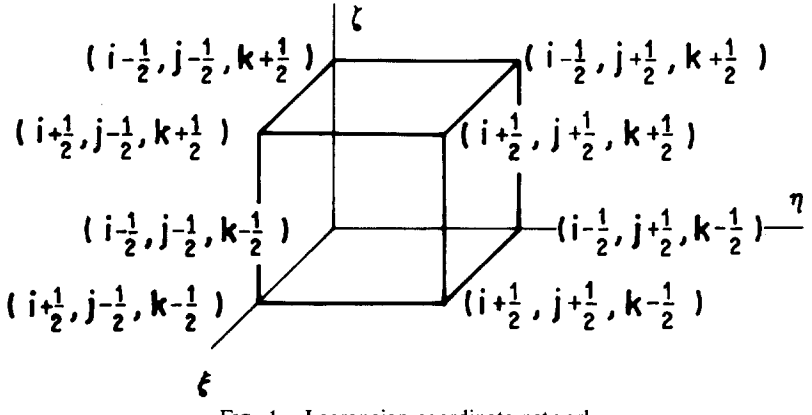

FIG. 1. Lagrangian coordinate network.

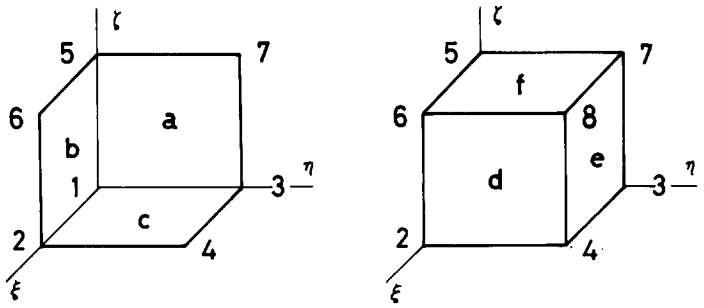

FIG. 2. Definition of vertices and surfaces for the cell (i, j, k).

— The mass density, velocity, and specific energy for the cell (i, j, k) are defined as $\rho_{i,j,k} = M_{i,j,k}/V_{i,j,k}$, $\mathbf{v}_{i,j,k} = \mathbf{P}_{i,j,k}/M_{i,j,k}$ and $e_{i,j,k} = U_{i,j,k}/M_{i,j,k}$, respectively. The specific internal energy is $\varepsilon_{i,j,k} = e_{i,j,k} - \frac{1}{2}\mathbf{v}^2_{i,j,k}$, and the pressure is given by an equation of state $p_{i,j,k} = p(\rho_{i,j,k}, \varepsilon_{i,j,k})$.

— Pressures and velocities are assumed constant along each cell surface.

Under these assumptions the following semidiscrete equations may be written

$$M\frac{d\mathbf{v}}{dt} = p_a\mathbf{S}_a + p_b\mathbf{S}_b + p_c\mathbf{S}_c - p_d\mathbf{S}_d - p_e\mathbf{S}_e - p_f\mathbf{S}_f \tag{6}$$

$$M\frac{de}{dt} = p_a\mathbf{v}_a\cdot\mathbf{S}_a + p_b\mathbf{v}_b\cdot\mathbf{S}_b + p_c\mathbf{v}_c\cdot\mathbf{S}_c - p_d\mathbf{v}_d\cdot\mathbf{S}_d - p_e\mathbf{v}_e\cdot\mathbf{S}_e - p_f\mathbf{v}_f\cdot\mathbf{S}_f \tag{7}$$

$$\frac{dV}{dt} = -\mathbf{v}_a\cdot\mathbf{S}_a - \mathbf{v}_b\cdot\mathbf{S}_b - \mathbf{v}_c\cdot\mathbf{S}_c + \mathbf{v}_d\cdot\mathbf{S}_d + \mathbf{v}_e\cdot\mathbf{S}_e + \mathbf{v}_f\cdot\mathbf{S}_f, \tag{8}$$

where M, $\mathbf{v}$, e, and V indicate $M_{i,j,k}$, $\mathbf{v}_{i,j,k}$, $e_{i,j,k}$, and $V_{i,j,k}$, respectively.

For the quantities associated with the surfaces a compatible choice (in the sense described below) is

$$\mathbf{v}_a\cdot\mathbf{S}_a = \mathbf{v}\cdot\mathbf{S}_a, \qquad \mathbf{v}_b\cdot\mathbf{S}_b = \mathbf{v}\cdot\mathbf{S}_b, \qquad \mathbf{v}_c\cdot\mathbf{S}_c = \mathbf{v}\cdot\mathbf{S}_c \tag{9}$$

and

$$p_d = p_e = p_f = p \tag{10}$$

(that means $\mathbf{v}_d\cdot\mathbf{S}_d = \mathbf{v}_{i+1,j,k}\cdot\mathbf{S}_d$, $p_a = p_{i-1,j,k}$, etc.). Then, Eqs. (6)–(8) reduce to

$$M\frac{d\mathbf{v}}{dt}=p_a\mathbf{S}_a+p_b\mathbf{S}_b+p_c\mathbf{S}_c-p(\mathbf{S}_d+\mathbf{S}_e+\mathbf{S}_f) \tag{11}$$

$$M\frac{de}{dt}=\mathbf{v}\cdot(p_a\mathbf{S}_a+p_b\mathbf{S}_b+p_c\mathbf{S}_c)$$
$$-p(\mathbf{v}_d\cdot\mathbf{S}_d+\mathbf{v}_e\cdot\mathbf{S}_e+\mathbf{v}_f\cdot\mathbf{S}_f) \tag{12}$$

$$\frac{dV}{dt}=-\mathbf{v}\cdot(\mathbf{S}_a+\mathbf{S}_b+\mathbf{S}_c)+\mathbf{v}_d\cdot\mathbf{S}_d+\mathbf{v}_e\cdot\mathbf{S}_e+\mathbf{v}_f\cdot\mathbf{S}_f. \tag{13}$$

Note the following properties:

— When Eqs. (11) to (13) are summed over the entire mesh only boundary terms remain.

— The specific internal energy becomes

$$M\frac{d\varepsilon}{dt}=M\frac{de}{dt}-\mathbf{v}\cdot M\frac{d\mathbf{v}}{dt}=-p\frac{dV}{dt} \tag{14}$$

(note that $\mathbf{S}_a+\mathbf{S}_b+\mathbf{S}_c=\mathbf{S}_d+\mathbf{S}_e+\mathbf{S}_f$). Equations (9) and (10) were called a compatible choice because they lead to Eq. (14).

Finally, for updating vertices positions, a possible choice is

$$\frac{d\mathbf{r}_1}{dt}=\mathbf{v}_{i,j,k} \tag{15.1}$$

$$\frac{d\mathbf{r}_2}{dt}=\mathbf{v}_{i+1,j,k}. \tag{15.2}$$

... ...

As it will be shown later, physical or geometrical reasons may require a better definition of vertices velocities (for instance, an appropriate mean value over neighbor cells). For each cell (i, j, k) three equations of motion (15.1), three of momentum (11), one of energy (12), and one for the volume (13) are solved (the surfaces are calculated through Eqs. (5.1)–(5.6)).

3. Boundary and Initial Conditions. Time Integration Method

Because of the "asymmetric" choice, Eqs. (9)–(10), the propagation of 3D waves in a uniform grid was studied. Let us consider a gas at rest with pressure p_0 and density ρ_0. The space is divided into N cartesian cells of equal mass M_0 and volume

$V_0 = \Delta x\, \Delta y\, \Delta z$. For a small perturbation, assuming $\mathbf{v} = \delta\mathbf{v}$, $p = p_0 + \delta p$ and $V = V_0 + \delta V$, Eqs. (11) and (13) become

$$M_0 \frac{d(\delta\mathbf{v})}{dt} = \mathbf{S}_a\, \delta p_a + \mathbf{S}_b\, \delta p_b + \mathbf{S}_c\, \delta p_c - (\mathbf{S}_d + \mathbf{S}_e + \mathbf{S}_f)\, \delta p \tag{16}$$

(note that $\delta\mathbf{S}_a + \delta\mathbf{S}_b + \delta\mathbf{S}_c - \delta\mathbf{S}_d - \delta\mathbf{S}_e - \delta\mathbf{S}_f = 0$)

$$\frac{d(\delta V)}{dt} = -(\mathbf{S}_a + \mathbf{S}_b + \mathbf{S}_c)\cdot\delta\mathbf{v} + S_d\cdot\delta\mathbf{v}_d + \mathbf{S}_e\cdot\delta\mathbf{v}_e + \mathbf{S}_f\cdot\delta\mathbf{v}_f. \tag{17}$$

Deriving Eq. (17) and neglecting second-order terms (i.e., terms proportional to $(d\mathbf{S}/dt)\cdot\delta\mathbf{v} \propto \mathbf{v}\cdot\delta\mathbf{v} \approx (\delta\mathbf{v})^2$),

$$\frac{d^2(\delta V)}{dt^2} = -(\mathbf{S}_a + \mathbf{S}_b + \mathbf{S}_c)\cdot\frac{d(\delta\mathbf{v})}{dt} + \mathbf{S}_d\cdot\frac{d(\delta\mathbf{v}_d)}{dt} + \mathbf{S}_e\cdot\frac{d(\delta\mathbf{v}_e)}{dt} + \mathbf{S}_f\cdot\frac{d(\delta\mathbf{v}_f)}{dt}. \tag{18}$$

For a γ-law gas, Eq. (14) leads to

$$\delta p = -\gamma p_0\, \delta V / V_0 \tag{19}$$

and, using Eq. (16), Eq. (18) becomes

$$\frac{d^2(\delta p_{i,j,k})}{dt^2} = \frac{\gamma p_0}{\rho_0}\left[\frac{\delta p_{i-1,j,k} - 2\delta p_{i,j,k} + \delta p_{i+1,j,k}}{(\Delta x)^2} + \frac{\delta p_{i,j-1,k} - 2\delta p_{i,j,k} + \delta p_{i,j+1,k}}{(\Delta y)^2} + \frac{\delta p_{i,j,k-1} - 2\delta p_{i,j,k} + \delta p_{i,j,k+1}}{(\Delta z)^2}\right], \tag{20}$$

where $\mathbf{S}_a = \mathbf{S}_d = (V_0/\Delta x)\hat{x}$, etc., and definitions (9)–(10) were used. Equation (20) indicates that pressure waves propagate in any direction at the same speed $c_s = (\gamma p_0/\rho_0)^{1/2}$.

For a general grid it is not possible to obtain an analytical result like Eq. (20). Anyway, some properties may be inferred. Note that Eqs. (11) to (13) are consistent; however, the wave equation does not reduce to the zero order differential equation in a non-uniform grid. For a one-dimensional case, a truncation error analysis gives an effective sound speed

$$c_s^2 = \frac{\gamma p_0}{\rho_0}\left(\frac{\delta a_i + \delta a_{i+1}}{2\delta a_i}\right), \tag{21}$$

where δa_i is the initial width of the ith cell (at $t = 0$).

A similar behavior is observed in other methods. For example, the one-dimensional lagrangian form of the method of Ref. [4] has an effective sound speed

$$c_s^2 = \frac{\gamma p_0}{\rho_0}\left(\frac{\delta a_{i-1} + 2\delta a_i + \delta a_{i+1}}{4\delta a_i}\right). \tag{22}$$

In this case, a way to overcome the problem is by choosing a different definition for the position of the cell center (the centers determine the vertices masses used in [4]). For a 1D problem it seems to be easy, but for a 3D case it is a difficult task.

Using the "asymmetric" choice it seems to be impossible to reduce the wave equation to a proper form even for a 1D case. Anyway, note that the error is determined by the initial mesh. That is, it is possible to estimate the error a priori. The reduction of the error has to be considered when constructing the initial mesh.

In conclusion, the "asymmetric" method treats waves with second-order accuracy on a regular mesh, but loss accuracy in a non-uniform mesh. A further discussion on the asymmetric behavior and the accuracy for one-dimensional problems will be given in the examples of Section 6.

The boundary and initial conditions for the semidiscrete equations are the same as those for the differential equations. For example, for barotropic fluids in fixed domains it is well known that there is at most one solution of the differential equations provided initial conditions for $\mathbf{v}$ and ρ are given at any point together with the boundary condition $\mathbf{v}$ on the contour at any time (provided no fluid is crossing the boundary). The same rule applies to the semidiscrete equations. Giving $\mathbf{v}$ on the boundary, the problem is solved. In particular, the pressure on the boundary is calculated from the results: giving for the "first" cell $\mathbf{v} = \mathbf{v}_a(t)$, the pressure p_a that is necessary to maintain $\mathbf{v} \cdot \mathbf{S}_a = \mathbf{v}_a \cdot \mathbf{S}_a$, i.e., p_a is calculated from the momentum equation (11), while giving $\mathbf{v}_d = \mathbf{v}_d(t)$ for the "last" cell, the pressure p_d is obtained from the energy equation (12) because $p_d = p$. Note that no phantom zones are needed. This is an advantage over centered methods that need phantom zones, because in the latter case, by choosing different boundary schemes it is possible to obtain different solutions [5]. Actually, this advantage is a characteristic of sided methods (e.g., [6]).

Regarding the time integration method, a necessary (but not always sufficient) condition is that it must provide a stable solution to Eqs. (16), (17), and (19).

Assuming a perturbation $\delta p = \delta p_0 \exp(\alpha t) \exp(ikx)$ and defining $\eta = \exp(\alpha \Delta t)$ and $A^2 = 2(c_s \Delta t/\Delta x)^2 [1 - \cos(k \Delta x)]$, it follows for an explicit scheme that

$$|\eta|^2 = 1 + A^2 > 1 \tag{23}$$

and therefore it is always unstable; while, for a fully implicit method

$$|\eta|^2 = \frac{1}{1 + A^2} < 1, \tag{24}$$

i.e., it is unconditionally stable.

After the explicit method, the simplest one is a predictor-corrector method as follows: a guess $\mathbf{x}_0^{n+1}$ (predictor) of $\mathbf{x}^{n+1}$ ($\mathbf{x}^{n+1}$ refers to any physical variable like pressure, velocity, etc., evaluated at the time $t+\Delta t$) is obtained explicitly from the values $\mathbf{x}^n$ at time t, using

$$\mathbf{x}_0^{n+1} = \mathbf{x}^n + \mathbf{h}(\mathbf{x}^n)\,\Delta t, \tag{25}$$

where

$$\mathbf{h}(\mathbf{x}) \equiv d\mathbf{x}/dt \tag{26}$$

and, finally, $\mathbf{x}^{n+1}$ is calculated from $\mathbf{x}_0^{n+1}$ using

$$\mathbf{x}^{n+1} = \mathbf{x}^n + \mathbf{h}(\mathbf{x}_0^{n+1})\,\Delta t. \tag{27}$$

For the perturbation described above, it follows from Eqs. (16), (17), and (19) that

$$|\eta|^2 = 1 - A^2 + A^4 \tag{28}$$

and the method is stable provided $A < 1$, that means CFL < 0.5. This criterion was used in the examples of Section 6 and no any further time step control was added. For all cases the calculation was started with the Δt given by the above condition.

4. Tensor Artificial Viscosity

Following Schulz [7] a tensor artificial viscosity is defined from three "one-dimensional" artificial viscosities in three different directions ($\mathbf{S}_d$, $\mathbf{S}_e$, and $\mathbf{S}_f$) as

$$q_d = \begin{cases} c^2\rho[\hat{n}_d\cdot(\mathbf{v}_d-\mathbf{v})]^2 & \text{if } \hat{n}_d\cdot(\mathbf{v}_d-\mathbf{v}) < 0 \\ 0 & \text{if } \hat{n}_d\cdot(\mathbf{v}_d-\mathbf{v}) \geqslant 0, \end{cases} \tag{29}$$

where q_d is the artificial viscosity term on face d, c is a dimensionless constant near unity, and $\hat{n}_d = \mathbf{S}_d/|\mathbf{S}_d|$. Similar definitions are used for q_e and q_f (q_a is equal to q_d of cell $(i-1, j, k)$, etc.).

Including the artificial viscosity, Eqs. (11) and (12) become

$$\begin{aligned} M\frac{d\mathbf{v}}{dt} = {} & p_a\mathbf{S}_a + p_b\mathbf{S}_b + p_c\mathbf{S}_c - p(\mathbf{S}_d + \mathbf{S}_e + \mathbf{S}_f) \\ & + q_a\mathbf{S}_a + q_b\mathbf{S}_b + q_c\mathbf{S}_c - q_d\mathbf{S}_d - q_e\mathbf{S}_e - q_f\mathbf{S}_f \end{aligned} \tag{30}$$

and

$$\begin{aligned} M\frac{de}{dt} = {} & \mathbf{v}\cdot(p_a\mathbf{S}_a + p_b\mathbf{S}_b + p_c\mathbf{S}_c) - p(\mathbf{v}_d\cdot\mathbf{S}_d + \mathbf{v}_e\cdot\mathbf{S}_e + \mathbf{v}_f\cdot\mathbf{S}_f) \\ & + (q_a\mathbf{S}_a + q_b\mathbf{S}_b + q_c\mathbf{S}_c)\cdot\mathbf{v} - q_d\mathbf{S}_d\cdot\mathbf{v}_d - q_e\mathbf{S}_e\cdot\mathbf{v}_e - q_f\mathbf{S}_f\cdot\mathbf{v}_f. \end{aligned} \tag{31}$$

The evolution of the internal energy is

$$M\frac{d\varepsilon}{dt} = -p\frac{dV}{dt} - q_a \mathbf{S}_a \cdot (\mathbf{v}_a - \mathbf{v}) - q_e \mathbf{S}_e \cdot (\mathbf{v}_e - \mathbf{v}) - q_f \mathbf{S}_f \cdot (\mathbf{v}_f - \mathbf{v}). \tag{32}$$

Note that the dissipation term introduced by the artificial viscosity is defined positive.

Another interesting feature is that only the rate of change of the volume that is caused by one surface overtaking another surface is considered rather than the total rate of change of volume [8].

Although this tensor artificial viscosity produces some errors in shocks crossing discontinuities (similar to that described in [9]) and they must be taken into consideration for a general application, in the examples of this work, it was not necessary to make any correction.

5. Reduction to One-Dimensional Equations

By choosing an appropriated cell structure it is possible to reduce the 3D equations to the 1D case. For example, consider a 1D problem with cylindrical geometry. Using a 3D grid in a Cartesian coordinate system as described in Fig. 3, as a result of the symmetry it is clear that

$$\mathbf{S}_e \cdot \mathbf{v}_e = \mathbf{S}_b \cdot \mathbf{v}_b \equiv \mathbf{S}_b \cdot \mathbf{v}; \qquad \mathbf{S}_f \cdot \mathbf{v}_f = \mathbf{S}_c \cdot \mathbf{v}_c \equiv \mathbf{S}_c \cdot \mathbf{v}; \qquad \mathbf{S}_c = \mathbf{S}_f \tag{33}$$

and

$$p_b = p_e \equiv p; \qquad p_c = p_f \equiv p; \qquad q_b = q_e; \qquad q_c = q_f. \tag{34}$$

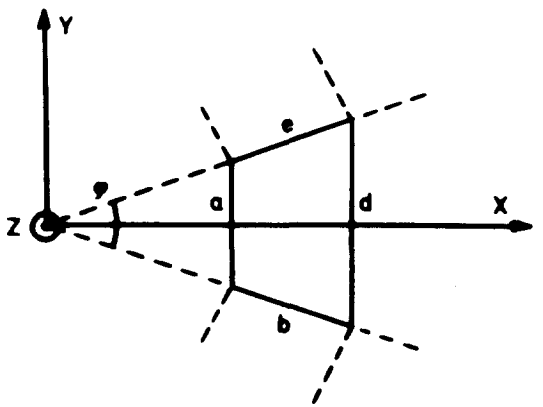

Fig. 3. Cell structure for calculating one-dimensional cylindrical problems using Cartesian coordinates.

Then, the momentum equation reduces to (only the cartesian x component is different from zero, i.e., the "radial" component)

$$M\frac{dv}{dt}=(p_a-p)S_a+(q_a-q_e)S_a-(q_d-q_e)S_d \tag{35}$$

(note that $\mathbf{S}_d+\mathbf{S}_e=\mathbf{S}_a+\mathbf{S}_b$; $\mathbf{S}_a=S_a\hat{x}$; $\mathbf{v}=v\hat{x}$; etc.) Further, when $\varphi \ll 1$ (see Fig. 3) then $q_e(\propto\varphi) \ll q_a, q_d$. Therefore, the above equation is written as

$$M\frac{dv}{dt}=(p_a-p)S_a+q_aS_a-q_dS_d. \tag{36}$$

The energy equation becomes

$$M\frac{de}{dt}=(p_a+q_a)S_av-(p+q_d)\,S_dv_d \tag{37}$$

and Eqs. (13), (15.1), and (29) reduce to

$$\frac{dV}{dt}=-S_av+S_dv_d \tag{38}$$

$$\frac{dr_1}{dt}=\frac{dr_a}{dt}=v \tag{39}$$

$$q_d=\begin{cases}c^2\rho(v_d-v)^2 & \text{if } v_d<v\\ 0 & \text{if } v_d\geqslant v.\end{cases} \tag{40}$$

Note that because of the use of a tensor artificial viscosity a proper expression for the sum of the "radial momentum" was obtained [7]; i.e., summing Eq. (36) over the entire mesh, the artificial viscosity vanishes completely from the equations as long as the q's are taken to be zero on the boundaries. This fact puts into evidence the difference between the tensor artificial viscosity and the scalar viscosity given in [10].

Finally, if an appropriate scaling on the mass and the volume is performed, it is easy to demonstrate that Eqs. (36) to (40) are valid for any 1D problem by defining

$$S_a=r_a^m, \tag{41}$$

where $m=0$, 1, 2 for planar, cylindrical, or spherical geometry, respectively, and the mass and volume are per unit area, per unit length and unit angle, and per unit solid angle, respectively.

6. Numerical Examples

In order to test the method several problems from 1D to 3D were solved. In all the examples the predictor-corrector method of Section 3 with CFL = 0.5 was used,

the artificial viscosity parameter was taken as $c = 1.3$, and the gas constant $\gamma = 1.4$. Programs (except the 28,000 mesh point example) were run in a personal computer PC-XT (8088, 10 Mhz, 640 Kbytes, with math coprocessor). Running time and memory requirements (in single precision, including all temporary storage needed) will be given for all the examples.

The first example is the same shock tube problem as Sod [11]. The tube extends from $x = 0$ to $x = 1$ and is divided into 100 computational cells uniformly distributed. In Fig. 4, pressure, density, and velocity are displayed as a function of the position at $t = 0.15$ (cycle 77) when the shock is located at $x \cong 0.75$.

Memory requirements are 40 bytes per cell and the running time per time step (cycle) was 0.38 s. Note that this time (obtained on a PC) is comparable to the running times given in [11] on a CDC 6600, and also to that from the MUSCL code [12] on a IBM 370/158.

The second example is the cylindrical propagation of a shock wave generated by an instantaneous energy release on a rigid cylindrical wall [13]. An equally spaced mesh with 70 cells was used. At $t = 0$ the energy per unit length of the cylinder, E_0, is deposited into the "last" cell (i.e., the closest to the wall) as internal energy, density is taken as ρ_0 and velocities are set to zero (the same dimensionless variables of Ref. [13] are used).

The boundary condition is $v = 0$ at any time along the cylinder wall (rigid wall). In Fig. 5, pressure, density, and velocity are shown as a function of the radius at the time the shock reaches the radius $R \cong 0.1$ ($t = 0.05$, cycle 286). Memory requirements are 40 bytes per cell and the running time is 0.21 s per cycle.

Due to the asymmetric form of Eq. (36) (S_a multiplies the pressure difference while S_d does not appear) the mesh was inverted, i.e., the S_a's were taken as the outer side of the cells. To do so a minus sign is added to definition (41) (because $\mathbf{S}_a = -S_a \hat{x}$) and inequalities in Eq. (40) are inverted (because $\hat{n}_d = -\hat{x}$). In Fig. 6a the pressure is shown at $t = 0.05$. Although a comparison with Fig. 5a gives a reasonable agreement (maximum relative differences of a few percent), in the second case some oscillations appear as a consequence of the asymmetric choices. Numerical experiments suggest that when a shock propagates from S_d to S_a it exhibits behavior better than that observed in a propagation from S_a to S_d.

Also a non-uniform mesh was tested. The pressure shown in Fig. 6b was obtained with an initial mesh given by $x^a_{i+1} = 1/N + x^a_i$, where $N = 70$ is the number of cells and $a = 1.5$. The agreement is excellent (compare to Fig. 5a).

Working with only 20 mesh points, good results were obtained (see Fig. 6c). The main difference is that, in this case, the shock is slower than the case $N = 70$: it reaches the position $R \cong 0.1$ at $t = 0.0545$.

All three cases of Fig. 6 provide essentially the same results with relative differences not bigger than 10%.

The third example is the flow at Mach 3 through a tunnel with a wedge. The height of the tunnel in the narrow part is H, the horizontal length of the wedge is $2H$, and the wedge angle is 15°. The geometry and the initial mesh with 910 cells (65×14) are depicted in Fig. 7. Initially the gas has a uniform pressure (p_∞) and

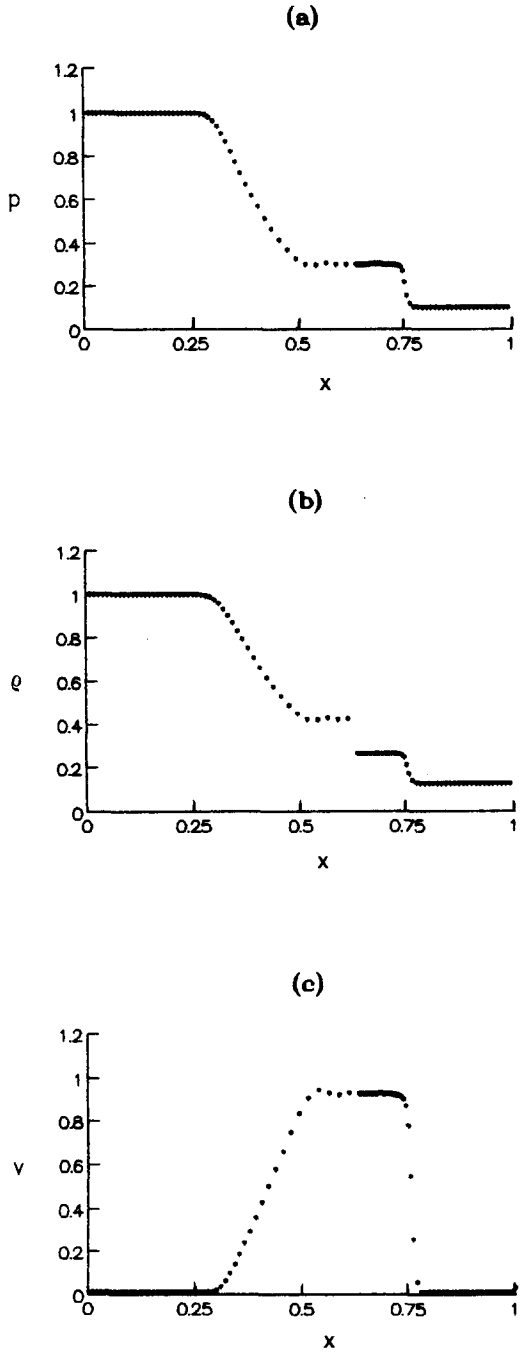

FIG. 4. Solution of the shock tube problem at $t = 0.15$ with $N = 100$: (a) pressure; (b) density; (c) velocity.

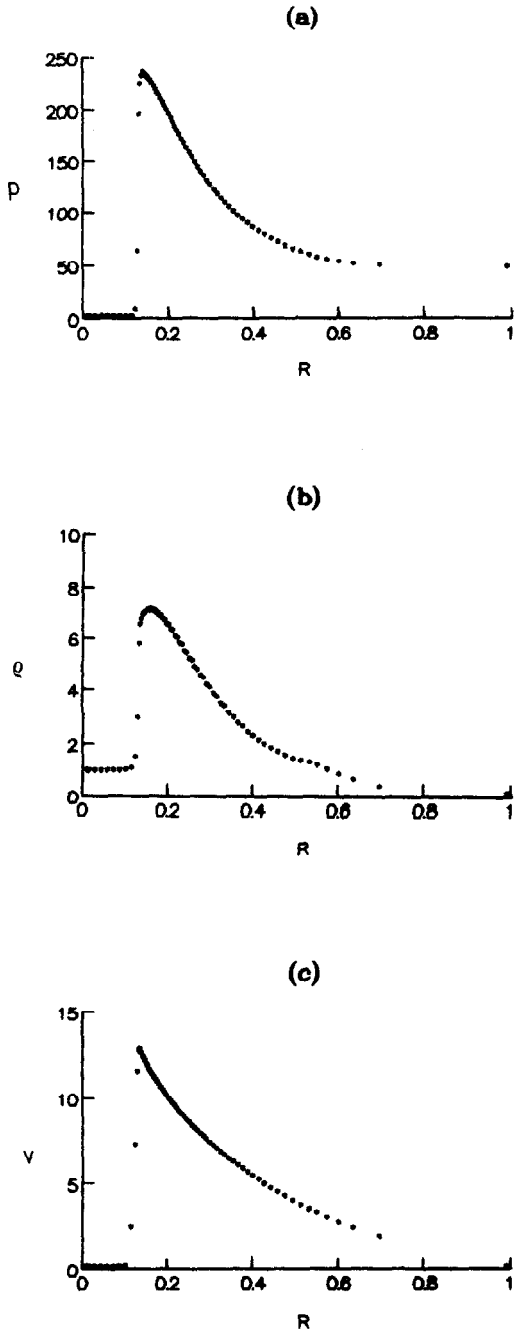

FIG. 5. Solution of the cylindrical propagation of a shock [13] at $t = 0.05$ with $N = 70$: (a) pressure (b) density; (c) velocity.

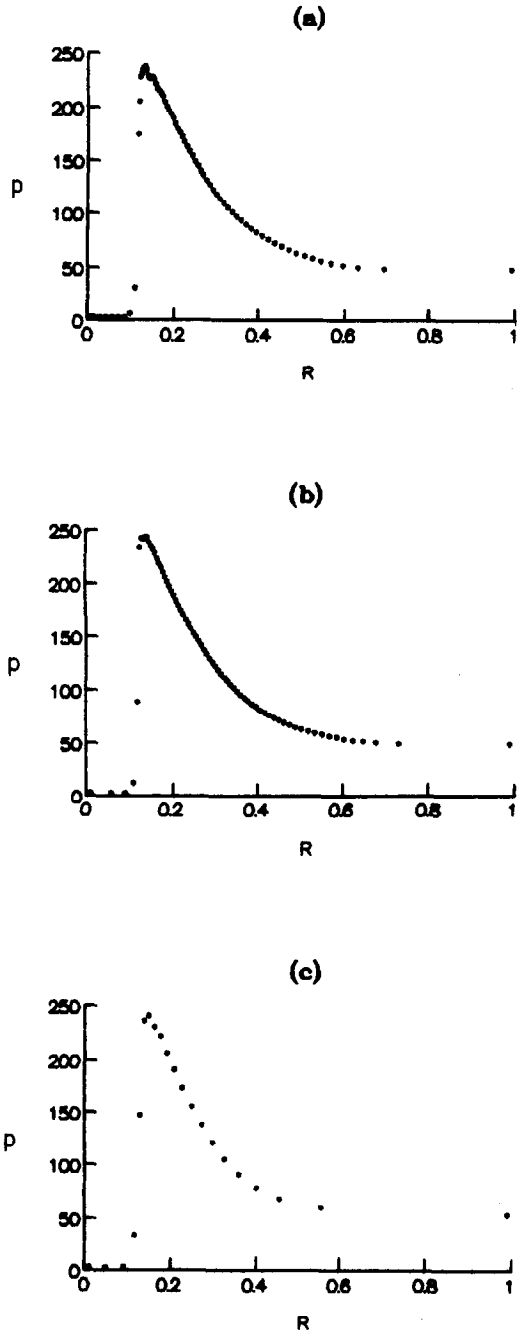

FIG. 6. Pressure as function of the position for the cylindrical propagation of a shock [13]: (a) $t = 0.05$, $N = 70$, inverted mesh (see text); (b) $t = 0.05$, $N = 70$, non-uniform mesh (see text); (c) $t = 0.0545$, $N = 20$, uniform mesh.

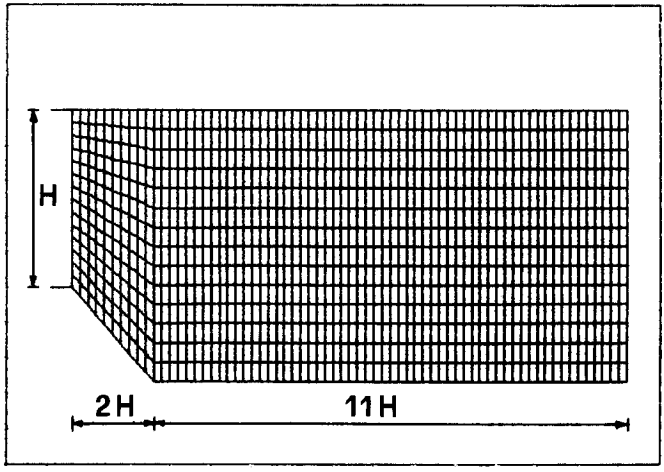

FIG. 7. Initial mesh (65 × 14) for the flow at Mach 3 through a tunnel containing a wedge. Wedge angle 15°.

at $t = 0$ the flow is impulsively started everywhere with an horizontal velocity $v = 3$ from right to left (Mach 3, $c_\infty = 1$).

Because of the use of a lagrangian method, the mesh is moving through the tunnel and some words about boundary conditions on the tunnel are in order. On the upper part it is easy to impose a free slip condition. On the lower boundary, cell vertices are forced to move on the boundary and the cells climb obstacles as depicted in Fig. 8. For these boundary cells, only the tangential component of the momentum equation is retained, projecting Eq. (30) onto the tangential direction. For each cell, the tangential direction ($\hat{\tau}$, see Fig. 8) is defined perpendicular to $\mathbf{S}_b$ and it may not coincide with the actual shape of the boundary. With this choice, $\mathbf{S}_b \cdot \mathbf{v} = 0$ and therefore p_b is not needed. After each cycle a new tangential velocity

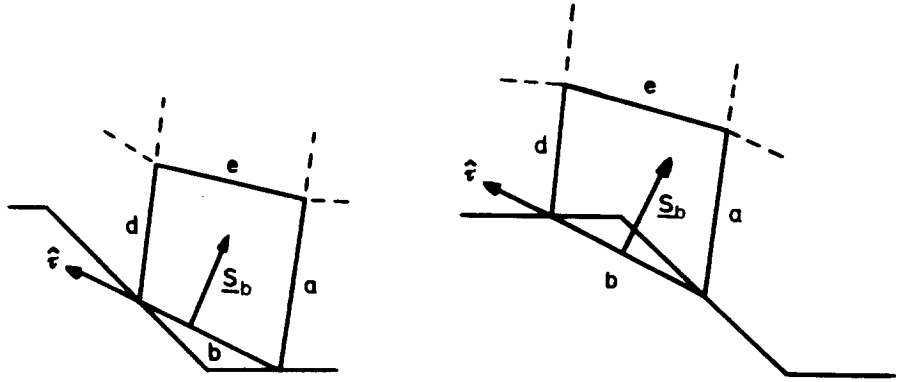

FIG. 8. A Lagrangian cell climbing an obstacle. The tangential direction $\hat{\tau}$ is defined perpendicular to $\mathbf{S}_b$.

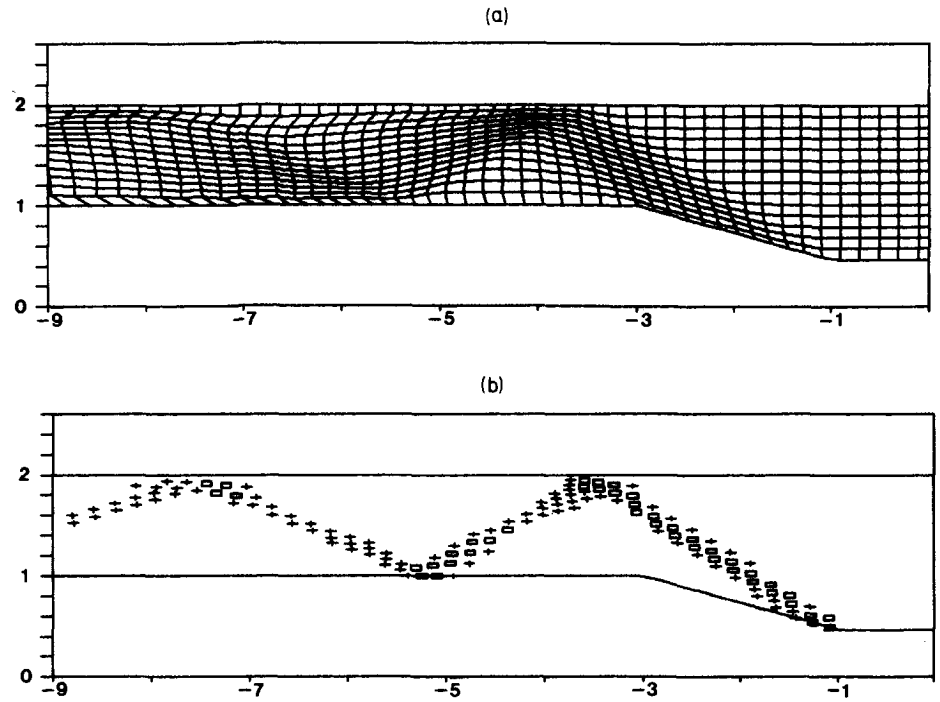

FIG. 9. (a) Mesh at $t = 3.5\, H/c_\infty$ for the flow at Mach 3 through a tunnel containing a wedge. (b) Shock position: □ cells with artificial viscosity $q_d + q_e > 0.1 p_\infty$, and + cells, where $q_d + q_e > 0.01 p_\infty$.

is obtained, and, from this, the corresponding tangential coordinate. The cartesian components are calculated from the new tangential direction defined by the new vertices positions. The boundaries at the left and right sides move at a constant velocity $v = 3$ from right to left.

In Fig. 9a the mesh is shown at $t = 3.5\, H/c_\infty$ (cycle 209) when practically the entire mesh has crossed the obstable. The shock position and its reflections are clearly depicted in Fig. 9b where cells with artificial viscosities $q_d + q_e > 0.1 p_\infty$ and $q_d + q_e > 0.01\, p_\infty$ are shown. Memory requirements are 57 bytes per cell and the running time was 7.7 s per cycle.

The last example is a 3D version of the second example. Figure 10 shows the initial mesh with 2000 cells ($20 \times 20 \times 5$) forming a pseudo-polar grid where i is the "radial" index, j the "azimutal" index, and k the "axial" index. The height of the cylinder is taken equal to its radius.

As in the second example, at $t = 0$ the energy per unit length of the cylinder, E_0, is deposited uniformly into the cells closest to the wall as internal energy, density is taken as ρ_0, and velocities are set to zero. The boundary condition is $\mathbf{v} = 0$ at any time along the cylinder wall (rigid wall). Initial volumes are calculated from node positions [14]. Finally, Eqs. (13), (15.1), (30), and (31) are solved in cartesian coordinates.

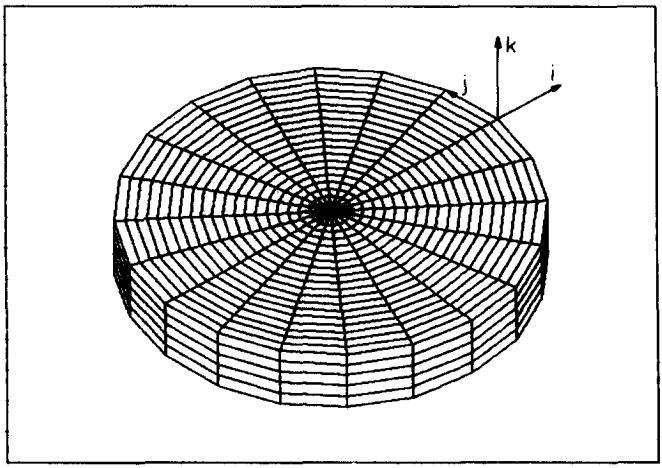

FIG. 10. Initial mesh ($20 \times 20 \times 5$) for the three-dimensional version of the cylindrical propagation of a shock.

Figure 11 shows the mesh at $t = 0.0545$ (cycle 61). As can be seen from the figure, there is a notable mesh distortion. This is due to the improper election of the vertices' velocities (Eq. (15.1)). This effect may be understood by looking at Fig. 12. In this case, a simple prescription may be done: replacing Eq. (15.1) by another containing an appropriate mean value, for example,

$$\frac{d\mathbf{r}_1}{dt} = \frac{1}{2}(\mathbf{v}_{i,j,k} + \mathbf{v}_{i,j-1,k}). \tag{42}$$

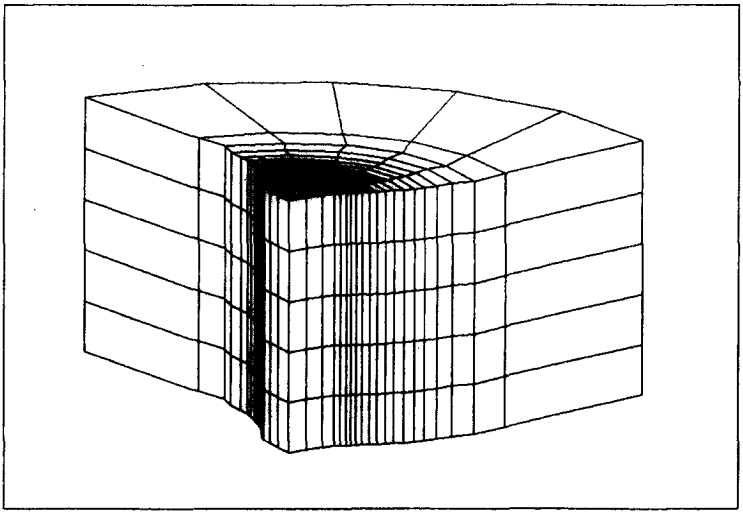

FIG. 11. Part of the mesh at $t = 0.0545$ for the cylindrical propagation of a shock showing the deformation produced by an improper definition of vertices velocities.

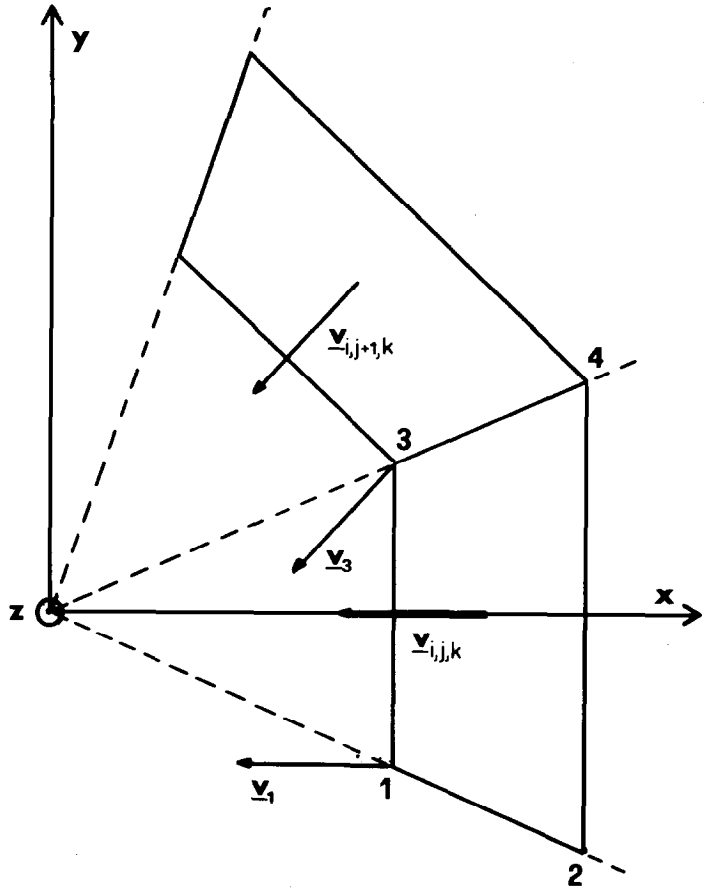

FIG. 12. Schematic demonstration of the cell distortion of Fig. 11 when the vertices velocities are taken as the cells velocities.

Figure 13 shows the mesh at the same time obtained using the above equation: the mesh distortion has disappeared.

It is important to note that the only difference between the solutions represented by Figs. 11 and 13 are the vertices' positions: the rest of the physical variables do not suffer from this distortion; i.e., the distortion does not affect seriously the results and/or the stability.

Figure 14a shows the mean density for each value of the "radial" index i as a function of R. For each i, the mean value is obtained by summing all possible values of j and k (100 points in this case). Also its dispersion is calculated. The maximum relative dispersion corresponding to Fig. 14a was 0.0013% for $i=4$. Memory requirements are 85 bytes per cell and running time was 40.1 s per cycle.

Using the same number of cells and the same "asymmetric" choice of variables,

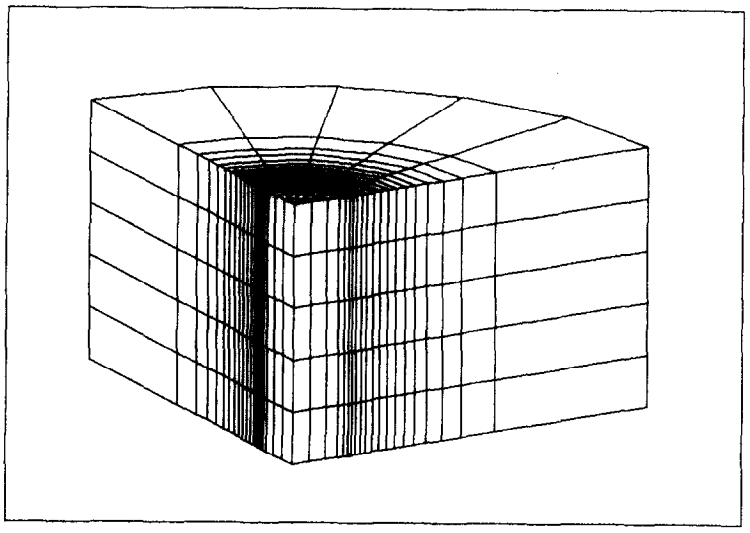

FIG. 13. Same solution as Fig. 11 but taken an appropriate mean value for vertices velocities (see text).

Eqs. (9)–(10), but the volume calculated from the vertices positions [14], a slightly different solution was obtained (see Fig. 14b), a bigger relative dispersion is observed (for $i=1$ it reaches 12%), and the calculation was $\cong 20\%$ slower because the volume equation of Ref. [14] requires more FLOPS than Eq. (13).

An attempt to use a symmetric choice that violates Eq. (14) (i.e., $p_a = \frac{1}{2}(p_{i,j,k} + p_{i-1,j,k})$, $\mathbf{v}_a = \frac{1}{2}(\mathbf{v}_{i,j,k} + \mathbf{v}_{i-1,j,k})$, etc.) and, using the same time integration method, ended in a "disaster": instabilities developed and the calculation was interrupted.

Increasing the number of cells from 2000 to 28,000 ($70 \times 40 \times 10$), a better convergence to the 1D solution is achieved. Figure 14c shows the mean density at $t=0.05$, practically the same as that obtained with the 1D code (see Fig. 5b). The maximum relative dispersion was 0.0026% for $i=10$.

7. CONCLUSIONS

Harlow [15] has pointed out that when adapting the differential equations to the discrete ones it is important to preserve, in first place, the physical principles that formed a basis for the equations. In the present work, by preserving the thermodynamic relation for internal energy (through the choice for the surface magnitudes given by Eqs. (9)–(10), i.e., the velocity from the cell "ahead" and the pressure from the cell "behind"), good results were obtained. The "asymmetric" choice led to a simple set of equations, where boundary conditions are easily

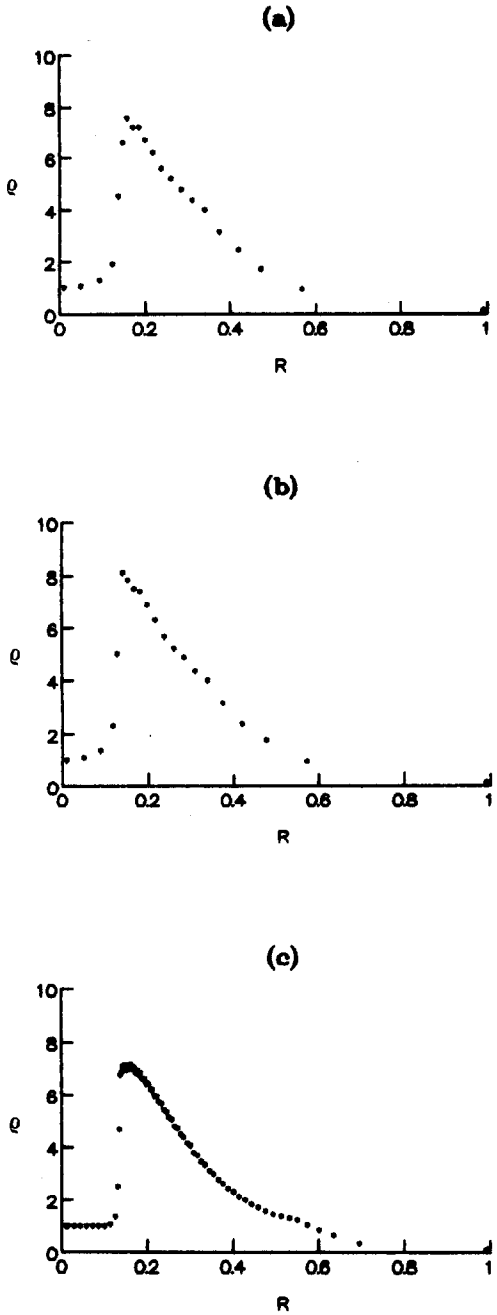

FIG. 14. Mean density as a function of the position for each value of the index i: (a) 2000 mesh point at $t = 0.0545$; (b) same as (a) but the volume being calculated from vertices position [14]; (c) 28,000 mesh point ($70 \times 40 \times 10$) at $t = 0.05$.

imposed and, together with a simple temporal integration scheme (a predictor-corrector method, explicitly predicted), a stable and fast code was written.

Although, in a non-uniform mesh the method is less accurate than other methods, it exhibits some important features: it retains the advantages of the sided methods over the centered ones for imposing boundary conditions, it preserves the simplicity of the explicit methods (a fact particularly useful to vectorize it), and it fits on a PC working with up to 6000 mesh points.

Finally, it is possible to use body-fitted coordinates [16] for defining the initial mesh and then integrating the equations in cartesian coordinates without needing coordinate transformations.

REFERENCES

1. A. A. AMSDEN AND C. W. HIRT, Los Alamos Scientific Laboratory Report LA-5100, 1973.
2. W. E. PRACHT AND J. U. BRACKBILL, Los Alamos Scientific Laboratory Report LA-6342, 1976.
3. A. A. AMSDEN AND H. RUPPEL, Los Alamos Scientific Laboratory Report LA-8905, 1981.
4. W. E. PRACHT, *J. Comput. Phys.* **17**, 132 (1975).
5. C. K. CHU AND A. SERENY, *J. Comput. Phys.* **15**, 476 (1974).
6. E. TURKEL, *Comput. Fluids* **11**, 121 (1983).
7. W. D. SCHULZ, "Two-Dimensional Lagrangian Hydrodynamics Difference Equations," in *Method of Computational Physics* edited by B. J. Adler, S. Fernbach, and M. Rotenberg (Academic Press, New York, 1964), Vol. III, p. 1.
8. M. L. WILKINS, *J. Comput. Phys.* **36**, 281 (1980).
9. I. G. CAMERON, *J. Comput. Phys.* **1**, 1 (1966).
10. J. VONNEUMANN AND R. D. RICHTMYER, *J. Appl. Phys.* **21**, 232 (1950).
11. G. A. SOD, *J. Comput. Phys.* **27**, 1 (1978).
12. B. VANLEER, *J. Comput. Phys.* **32**, 101 (1979).
13. H. MATSUO, Y. OHYA, K. FUJIWARA, AND H. KUDOH, *J. Comput. Phys.* **75**, 384 (1988).
14. J. K. DUKOWICZ, *J. Comput. Phys.* **74**, 493 (1988).
15. F. HARLOW, Los Alamos Scientific Laboratory Report LA-DC-9996, 1970.
16. F. C. THAMES, J. F. THOMPSON, C. W. MASTIN, AND R. L. WALKER, *J. Comput. Phys.* **24**, 245 (1977).